JCTC Journal of Chemical Theory and Computation

Gaussian Multipole Model (GMM)

Dennis M. Elking,[†] G. Andrés Cisneros,[†] Jean-Philip Piquemal,[‡] Thomas A. Darden,[†] and Lee G. Pedersen*[,†,§]

Laboratory of Structural Biology, National Institute of Environmental Health Sciences, P.O. Box 12233, MD K3-16, Research Triangle Park, North Carolina 27709, Laboratoire de Chimie Théorique, UMR 7616 CNRS, Université Pierre-et-Marie-Curie, Case Courier 137, 4, Place Jussieu, 75252 Paris, France, and University of North Carolina, Department of Chemistry, Chapel Hill, North Carolina 27599

Received July 9, 2009

Abstract: An electrostatic model based on charge density is proposed as a model for future force fields. The model is composed of a nucleus and a single Slater-type contracted Gaussian multipole charge density on each atom. The Gaussian multipoles are fit to the electrostatic potential calculated at the B3LYP/6-31G* and HF/aug-cc-pVTZ levels of theory and tested by comparing electrostatic dimer energies, intermolecular density overlap integrals, and permanent molecular multipole moments with their respective ab initio values. For the case of water, the atomic Gaussian multipole moments Q_{lm} are shown to be a smooth function of internal geometry (bond length and angle), which can be approximated by a truncated linear Taylor series. In addition, results are given when the Gaussian multipole charge density is applied to a model for exchange−repulsion energy based on the intermolecular density overlap.

1. Introduction

Force fields are routinely used to simulate biological molecules in order to study structure and function. Recently, attention has been focused on developing accurate force field models that are able to provide a more realistic account of intermolecular interactions. For example, polarization models[1−6] have been incorporated into force fields[7−16] in order to account for many-body effects[17−20] in polar environments. In the SIBFA[10−12] force field, multipoles are placed on atoms and bond barycenters in order to accurately account for the anisotropy in electrostatic interactions. AMOEBA[13−16] places multipoles on atoms and has been developed as a force field for protein simulations. In addition, electrostatic models, which employ geometry-dependent charges, are being investigated.[21−24]

Atomic point multipole models derived from distributed multipole expansions[25−28] or fit to the electrostatic potential[29] (ESP) have been proposed to improve the description of electrostatic interactions. However, at short-range, it has been noted[25,30,31] that atomic point multipole electrostatic models significantly underestimate electrostatic interactions at dimer distances. This effect, called penetration error, becomes important at dimer distances where there is significant overlap of molecular charge densities. Damping functions[31−34] have been proposed as a short-range correction to atomic point multipoles in order to account for penetration effects.

Another approach for calculating short-range electrostatic interactions has been to model the electron density. For example, simple Gaussian charge densities[35−37] have been used in models for liquids. Wheatley[38,39] has studied Cartesian Gaussian multipole charge distributions,[40,41] which are obtained by differentiating simple normalized Gaussian functions. It was shown that at long-range, the interactions between Gaussian multipole charge densities behave asymptotically as point multipoles.[38] As an example, consider a Cartesian Gaussian dipole charge distribution ρ_μ with dipole moment $\vec{\mu}$, exponent α, and nuclear center $\vec{R}$ given by

* Corresponding author.lee_pedersen@unc.edu.

[†] Laboratory of Structural Biology, National Institute of Environmental Health Sciences.

[‡] Laboratoire de Chimie Théorique, Université Pierre-et-Marie-Curie.

[§] University of North Carolina, Department of Chemistry.

10.1021/ct900348b
Published on Web 11/23/2009

$$\rho_\mu(\vec{r}) \equiv \vec{\mu}\cdot\nabla_R\left(\frac{\alpha^2}{\pi}\right)^{3/2}\exp(-\alpha^2|\vec{r}-\vec{R}|^2) \quad (1)$$

where $\vec{r}$ is the field point and ∇_R is the Cartesian gradient with respect to the nuclear center $\vec{R}$. The electrostatic potential $\phi_\mu(\vec{r})$ arising from ρ_μ is given by

$$\phi_\mu(\vec{r}) = \int d^3r' \frac{\rho_\mu(\vec{r}')}{|\vec{r}-\vec{r}'|} = \vec{\mu}\cdot\nabla_R\frac{\mathrm{erf}(\alpha|\vec{r}-\vec{R}|)}{|\vec{r}-\vec{R}|} \quad (2)$$

where erf(x) is the error function defined by

$$\mathrm{erf}(x) \equiv \frac{2}{\sqrt{\pi}}\int_0^x \exp(-u^2)du \quad (3)$$

Note that for large x, erf(x) ≈ 1. Thus, for large exponents or separations, the electrostatic potential arising from a Gaussian dipole behaves as a point dipole, i.e.

$$\phi_\mu(\vec{r}) \approx \vec{\mu}\cdot\nabla_R\frac{1}{|\vec{r}-\vec{R}|} \qquad \alpha|\vec{r}-\vec{R}| >> 1 \quad (4)$$

Recently, Giese and York[42] have derived the electrostatic energy integral, the density overlap integral, and the gradients of their matrix elements between contracted solid harmonic Gaussian (multipole) charge densities in the spherical tensor framework. In analogy to taking derivatives of simple normalized Gaussian functions to create Cartesian Gaussian multipoles, spherical tensor Gaussian multipoles can be constructed by contracting spherical tensor multipole moments Q_{lm} with the solid harmonic gradient operator[43,44] $C_{lm}(\nabla)$ acting upon a simple Gaussian function. In the Supporting Information, a summary of the mathematical background[43−47] used in this work, including definitions and theorems for the solid harmonic function $C_{lm}(x, y, z)$ and the solid harmonic gradient operator $C_{lm}(\nabla)$, is provided.

Methods of calculating the Gaussian charge density parameters are also being explored. Previously, we have proposed the Gaussian Electrostatic Model (GEM)[10,48−51] as an electrostatic model based on Gaussian charge density. The GEM density $\rho(r)$ is represented by a linear expansion of conventional auxiliary Gaussian basis sets. The density coefficients are fit to the ab initio density $\rho^{\mathrm{QM}}(r)$ through a least-squares fit to the error in self-interaction electrostatic energy[52−56] ΔE_{self} given by

$$\Delta E_{\mathrm{self}} = \langle\rho^{\mathrm{QM}}(r) - \rho(r)|\frac{1}{r}|\rho^{\mathrm{QM}}(r) - \rho(r)\rangle \quad (5)$$

GEM has been shown to accurately reproduce intermolecular electrostatic interaction energies at both short- and long-range distances. In addition, it was also shown that a GEM-type model can be constructed by fitting to the electrostatic potential (ESP) numerically on a grid.[57] When fitting to ESP, it was found that fewer Gaussian basis functions were needed to reproduce ab initio intermolecular electrostatic energies as compared to fitting to the error in self-interaction electrostatic energy ΔE_{self}. In that work, we have also given some preliminary results for fitting a single s-type Gaussian charge function on each atom to the ESP. It was found that a simple model consisting of a single negative Gaussian charge distribution and positive nucleus on each atom is able to account for a large fraction of the penetration error and that it represents a significant improvement over atomic point charge models for short-range electrostatic interactions.

In the present study, we propose a natural extension to the single (uncontracted) s-type Gaussian charge model by generalizing to a model based on a single diffuse contracted Gaussian multipole charge density on each atom. The radial part of the Gaussian multipole charge density is a Slater-type[58,59] contracted Gaussian function fit to exp(-λr). For each atom, the Gaussian multipole moments Q_{lm} and a single Slater-type exponent parameter λ are fit to the ESP surrounding the molecule calculated at the B3LYP/6-31G* or HF/aug-cc-pVTZ levels of theory. The model is tested by comparing electrostatic dimer energies, intermolecular density overlap integrals, and permanent molecular moments with their reference ab initio values. In addition, a significantly improved method of fitting the Gaussian multipoles to the ESP numerically on a grid is adopted. In particular, angular grids available in most quantum chemistry codes are used, and a smooth weighting function, similar to the one proposed by Hu[60] et al., is used to filter out points near the nuclear centers.

In this work, we will show that a single diffuse contracted Gaussian multipole (shell) on each atom is capable of reproducing ab initio intermolecular electrostatic energies and density overlap integrals on hydrogen-bonded dimers at equilibrium geometries. For intermolecular electrostatic energies, the accuracy attained by Gaussian multipoles is shown to be approximately 0.1 kcal/mol, which is comparable to that of our original GEM model. Since the GEM model is represented by an auxiliary Gaussian basis set consisting of many uncontracted Gaussian shells (multipoles) on each atom, the proposed single Gaussian multipole model is expected to be an efficient model suitable for developing a force field for molecular dynamics simulations. In addition, since there are fewer fitted parameters used in Gaussian multipoles, the fit is more stable. Based on this property, the atomic Gaussian multipoles Q_{lm} are shown to be a continuous function of internal geometry (bond lengths and angles, etc). More specifically, it is shown that the atomic Gaussian multipole moments Q_{lm} can be approximated as a truncated linear Taylor series in both bond length and angle for the case of water.

The intermolecular density overlap integral calculated by Gaussian multipoles can be applied to the exchange−overlap model proposed by Wheatley and Price[61,62] for the exchange−repulsion energy. The first order intermolecular exchange−repulsion energy E_{exch} is defined as the total ab initio dimer energy minus the intermolecular electrostatic energy calculated using the frozen monomer wave functions. The ab initio exchange−repulsion energy E_{exch} can be modeled by fitting a proportionality constant K to the intermolecular density overlap integral S by

$$E_{\mathrm{exch}} \cong KS^a \quad (6)$$

where a is an empirical exponent parameter used to improve the quality of fit.[62] The expression in eq 6 is commonly generalized to a pairwise sum over atom−atom[61,62] contributions between the two monomers. One of the challenges of developing parameters and applying the exchange−overlap

model is first finding an accurate and convenient representation of the molecular charge density. In a previous work,[48,50] we have applied the exchange−overlap model in eq 6 to the GEM molecular charge density. A molecular pair K parameter was fit to the ab initio exchange−repulsion energy for the water−water dimer over several randomly oriented water−water geometries. Although fitting molecular pair K parameters over atomic pair parameters may not be ideal for constructing a general force field, we are interested in studying the effects of applying an anisotropic charge density to the exchange−overlap model. In the present study, a single molecular pair K parameter (eq 6) is fit to the ab initio exchange energies using the intermolecular density overlap integrals calculated by atomic Gaussian monopoles, dipoles, and quadrupoles for small molecule hydrogen-bonded dimers. Including anisotropy in the description of charge density is shown to make a significant improvement in reproducing ab initio exchange−repulsion energies.

In the following section, a Gaussian multipole charge density is defined, and expressions for the electrostatic potential, the electrostatic energy, and the density overlap integral are given. Details on fitting Gaussian multipoles to the electrostatic potential are provided along with a discussion on how the model is tested with ab initio intermolecular electrostatic energies, intermolecular density overlap integrals, and permanent molecular multipole moments. This is followed by a brief discussion on how the intermolecular density overlap integrals calculated by Gaussian multipoles are applied to the exchange−overlap model. In the next section, results for Gaussian multipoles are presented. Intermolecular electrostatic energies, intermolecular density overlap integrals, and permanent molecular multipole moments calculated by Gaussian multipoles are compared with their respective ab initio values. The geometry dependence of atomic Gaussian multipole moments Q_{lm} is presented for the case of water. Results are given when the Gaussian multipole intermolecular density overlap integrals are applied to the exchange−overlap model. Lastly, the results are summarized and future applications are discussed in the Conclusion Section.

2. Methods

In this section, a definition of a contracted Gaussian multipole charge density is given along with expressions for the electrostatic potential, electrostatic energy, and density overlap integrals. This is followed by a brief discussion of Slater-type contracted Gaussian functions and a description of how the Gaussian multipoles are fit to the ESP. In the next subsection, computational details on the calculation of ab initio electrostatic energies and intermolecular density overlap integrals are discussed. The calculation of permanent molecular multipole moments are described. This section concludes with computational details of how the exchange−overlap parameters are fit.

2.1. Gaussian Multipoles. The definition we have used for a contracted Gaussian multipole charge density is similar to the one given by Giese and York.[42] In that work,[42] expressions for efficiently calculating electrostatic and density overlap matrix element integrals between real regular solid harmonic contracted Gaussian functions are given along with gradients of their matrix elements. In order to test the model for Gaussian multipole charge density, we have implemented similar expressions using complex solid harmonic Gaussian (multipole) functions, which are given below. A derivation of the following results along with a summary of necessary mathematical background[43−47] are given in the Supporting Information for the interested readers. Many of the theorems quoted in the Supporting Information have been used in the evaluation of integrals between solid harmonic Gaussian basis functions[63−65] for quantum chemistry calculations.

In the Introduction, it was mentioned that a spherical tensor Gaussian multipole charge distribution can be defined in terms of multipole moments Q_{lm} and of the solid harmonic gradient operator $C_{lm}(\nabla)$ acting upon a normalized Gaussian function. As shown in the Supporting Information, the solid harmonic gradient operator is especially useful in deriving integral quantities, such as electrostatic energies and density overlap integrals. In the following discussion, the final results for the electrostatic energy and the overlap integral between two Gaussian multipole charge densities are given after all derivative operations have been evaluated.

A contracted Gaussian multipole charge density $\rho(\vec{r},\vec{R})$ with moments Q_{lm} and nuclear center $\vec{R}$ evaluated at the point $\vec{r}$ is given by

$$\rho(\vec{r},\vec{R}) \equiv \sum_{l=0}^{l_{\max}} \sum_{|m|\le l} \frac{Q_{lm} C_{lm}^{*}(\vec{r}-\vec{R})}{(2l-1)!!} \rho_l(|\vec{r}-\vec{R}|;\alpha_\mu) \tag{7}$$

where $l_{\max}$ is the maximum order of the Gaussian multipoles (e.g., $l_{\max} = 0$ for monopoles, 1 for dipoles, etc.), C_{lm}^{*} is the complex conjugate of a solid harmonic function, and ρ_l is a derivative of a contracted Gaussian charge density defined by

$$\rho_l(r;\alpha_\mu) \equiv \left(-\frac{1}{r}\frac{d}{dr}\right)^l \sum_{\mu=1}^{N_C} c_\mu \left(\frac{\alpha_\mu^2}{\pi}\right)^{3/2} \exp(-\alpha_\mu^2 r^2) \tag{8}$$

where N_c is the degree of contraction. For $l = 0$, the density ρ_0 is normalized to unity, ($\sum_\mu c_\mu = 1$). The multipole moments of the charge density $\rho(\vec{r},\vec{R})$ with respect to the center $\vec{R}$ are the coefficients Q_{lm}, i.e.

$$\int d^3 r \rho(\vec{r},\vec{R}) C_{lm}(\vec{r}-\vec{R}) = Q_{lm} \tag{9}$$

The electrostatic potential ϕ arising from ρ in eq 7 is given by

$$\begin{aligned}\phi(\vec{r}) &= \int d^3 r' \frac{\rho(\vec{r}',\vec{R})}{|\vec{r}-\vec{r}'|} \\ &= \sum_{l=0}^{l_{\max}} \sum_{|m|\le l} \frac{Q_{lm} C_{lm}^{*}(\vec{r}-\vec{R})}{(2l-1)!!} \phi_l(|\vec{r}-\vec{R}|;\alpha_\mu)\end{aligned} \tag{10}$$

where $\phi_l$is defined by

$$\phi_l(r;\alpha_\mu) \equiv \left(-\frac{1}{r}\frac{d}{dr}\right)^l \sum_{\mu=1}^{N_C} c_\mu \frac{\mathrm{erf}(\alpha_\mu r)}{r} \tag{11}$$

and erf(x) is the error function defined in eq 3.

The electrostatic interaction energy between two Gaussian multipole charge densities $\rho_1(\vec{r},\vec{R}_1)$ and $\rho_2(\vec{r},\vec{R}_2)$ and their nuclei Z_1 and Z_2 is given by

$$U = \int\int d^3r d^3r' \frac{\rho_1(\vec{r},\vec{R}_1)\rho_2(\vec{r}',\vec{R}_2)}{|\vec{r} - \vec{r}'|} + Z_1\phi_2(\vec{R}_1) + Z_2\phi_1(\vec{R}_2) + \frac{Z_1Z_2}{|\vec{R}_1 - \vec{R}_2|} \quad (12)$$

where $\phi_2(\vec{R}_1)$ is the potential at $\vec{R}_1$ due to ρ_2 and $\phi_1(\vec{R}_2)$ is defined by a similar expression. The density overlap integral S between two Gaussian multipole charge densities is defined by

$$S = \int d^3r \rho_1(\vec{r})\rho_2(\vec{r}) \quad (13)$$

The electrostatic and density overlap integrals in eqs 12 and 13 can be expressed by[42]

$$\int\int d^3r d^3r' \rho_1(\vec{r})O(\vec{r},\vec{r}')\rho_2(\vec{r}') = \sum_{l_1,m_1}\sum_{l_2,m_2} Q^1_{l_1m_1}T_{l_1m_1;l_2m_2}Q^2_{l_2m_2} \quad (14)$$

where $O(\vec{r},\vec{r}') \equiv 1/|\vec{r} - \vec{r}'|$ for the electrostatic integral, $O(\vec{r},\vec{r}') \equiv \delta(\vec{r} - \vec{r}')$ for the density overlap integral, and the interaction matrix $T_{l_1m_1;l_2m_2}$ is given below. The electrostatic energy and density overlap integrals between two normalized contracted Gaussian monopole charge densities with unit charge are given by

$$F_0(R) \equiv \sum_{\mu,\nu} c^1_\mu c^2_\nu \frac{\mathrm{erf}(\alpha_{\mu\nu}R)}{R} \quad (15a)$$

$$F_0(R) \equiv \sum_{\mu,\nu} c^1_\mu c^2_\nu \left(\frac{\pi}{\alpha^2_{\mu\nu}}\right)^{3/2} \exp(-\alpha^2_{\mu\nu}R^2) \quad (15b)$$

where R is the distance between nuclear centers and α_μ is the Gaussian product exponent defined by

$$R \equiv |\vec{R}_1 - \vec{R}_2| \qquad \alpha_{\mu\nu} \equiv \frac{\alpha_\mu\alpha_\nu}{\sqrt{\alpha^2_\mu + \alpha^2_\nu}} \quad (16)$$

In addition, the constants A_{lm} and B_{lm} are defined by

$$A_{lm} \equiv \sqrt{(l+m)!(l-m)!}, \qquad B_{lm} \equiv \frac{A_{lm}}{(2l-1)!!} \quad (17)$$

for $l \neq 0$, and $A_{00} = B_{00} = 1$. The scaled solid harmonic function is defined by $R_{lm}(\vec{r}) \equiv C_{lm}(\vec{r})/A_{lm}$. The interaction matrix $T_{l_1m_1;l_2m_2}$ from eq 14 is given by

$$T_{l_1m_1;l_2m_2} = B_{l_1m_1}B_{l_2m_2}\sum_{l=0}^{\min(l_1,l_2)}\sum_{m=-l}^{l}\frac{(-1)^{l_2+m}}{A_{lm}B_{lm}} \times R^*_{l_2-l,m_2+m}(\vec{R})R^*_{l_1-l,m_1-m}(\vec{R})F_{l_2+l_1-l}(R) \quad (18)$$

where $F_l(R) \equiv 2^l\,(d/\mathrm{d}R^2)^l\,F_0(R)$. Finally, the point multipole results for both electrostatic potential and energy can be found by considering an uncontracted Gaussian multipole ($N_c = 1$), taking the large exponent limit ($\alpha \rightarrow \infty$) and noting $\mathrm{erf}(x) \rightarrow 1$ as $x \rightarrow \infty$.

The atomic Gaussian multipole moments Q_{lm} are commonly defined[25] with respect to a local frame of the atom Q^{local}_{lm} and then rotated to a system or global frame $Q^{\mathrm{global}}_{lm} \equiv Q_{lm}$ through Wigner rotation matrices $\mathbf{D}^l_{m'm}$

$$Q^{\mathrm{global}}_{lm} = \sum_{m'} \mathbf{D}^l_{m',m}[\mathbf{R}^{-1}]Q^{\mathrm{local}}_{lm'} \quad (19)$$

Recursion formulas for evaluating $\mathbf{D}^l_{m'm}$ have been given in Choi[66] et al. For each atom, the Cartesian transformation matrix $\mathbf{R}$ between the local and global frames is defined with respect to the relative positions of the atom and of its neighbors.[13,67,68]

2.2. Slater-Type Contracted Gaussian functions. The contraction coefficients d_μ and exponents α_μ are fit to a simple Slater function $\exp(-r)$ over all space for $N_c = 1 - 14$

$$\exp(-r) \cong \sum_{\mu=1}^{N_C} d_\mu \exp(-\alpha^2_\mu r^2) \quad (20)$$

For $N_c = 1 - 6$, the optimized exponents agree with those used in the development of the original STONG basis sets.[58,59] The contraction coefficients d_μ and exponents α_μ fit to $\exp(-r)$ are used to find the corresponding coefficients and exponents for $\exp(-\lambda r)$ by a scaling argument. The final expression for a normalized Slater-type charge density with unit charge and with exponent λ is given by

$$\frac{\lambda^3}{8\pi}\exp(-\lambda r) \cong \sum_{\mu=1}^{N_C} c_\mu \left(\frac{\alpha^2_\mu\lambda^2}{\pi}\right)^{3/2} \exp(-\alpha^2_\mu\lambda^2 r^2) \quad (21)$$

where $c_\mu \equiv d_\mu/8\pi \times (\pi/\alpha^2_\mu)^{3/2}$. A full list of contracted coefficients and exponents for $\exp(-r)$ can be found in the Supporting Information for $N_c = 1 - 14$.

2.3. Nonlinear Fit to Potential. The model for molecular charge density presented in this work consists of an effective nuclear charge Z_{eff} and a set of contracted Gaussian multipole moments Q_{lm} with a single diffuse Slater exponential parameter λ centered on each atom. Only the valence charge density is modeled, and the core electron density near the nuclear centers is neglected by using screened nuclear charges $Z_{\mathrm{eff}} = Z - N_{\mathrm{core}}$, where Z is the true nuclear charge and N_{core} is the number of core electrons. The number of core electrons N_{core} is taken to be 0 for hydrogen, 2 for the first-row elements, and 10 for the second-row elements. Thus, the screened nuclear charges Z_{eff} are set to 1.0 for H, 4.0 for C, 5.0 for N, 6.0 for O, 7.0 for F, and 7.0 for Cl. Initially, we experimented with using the true nuclear charges, e.g. $Z = 8$ for O. However, when the true nuclear charges are used, the intermolecular density overlap integrals at equilibrium dimer distances are consistently overestimated by 10−15%. If the true nuclear charges are used, then the model is forced to account for both the core and valence electron density with a single diffuse Slater-type Gaussian function. By only modeling the valence charge density, we had found that using effective screened nuclear charges gave significantly smaller errors when comparing to the ab initio intermolecular electrostatic energy and the density overlap integral.

The model for Gaussian multipole molecular charge density ρ^{GM} evaluated at the point $\vec{r}$ is represented as a sum over atomic Gaussian multipole charge densities given by

$$\rho^{\mathrm{GM}}(\vec{r}) = \sum_{a} \sum_{l=0}^{l_{\max}} \sum_{|m|\le l} \frac{Q_{lm,a} C^{*}_{lm}(\vec{r} - \vec{R}_a)}{(2l-1)!!} \rho_l(|\vec{r} - \vec{R}_a|; \lambda_a \alpha_\mu) \tag{22}$$

where $\vec{R}_a$ is the nuclear center of atom a, $Q_{lm,a}$ is the atomic Gaussian multipole moments of atom a, λ_a is the Slater exponent on atom a, and ρ_l is defined by eq 8. The electrostatic potential due to the effective nuclear charges and the Gaussian multipole charge density can be found from eq 10 as

$$\phi(\vec{r}; Q_{lm,a}, \lambda_a) = \sum_{a} \frac{Z_{\mathrm{eff},a}}{|\vec{r} - \vec{R}_a|} + \sum_{l=0}^{l_{\max}} \sum_{|m|\le l} \frac{Q_{lm,a} C^{*}_{lm}(\vec{r} - \vec{R}_a)}{(2l-1)!!} \phi_l(|\vec{r} - \vec{R}_a|, \lambda_a \alpha_\mu) \tag{23}$$

where $\vec{r}$ is the field point, $Z_{\mathrm{eff},a}$ is the effective nuclear charge of atom a, and ϕ_l is defined by eq 11. For each atom, $Q_{lm,a}$ and λ_a are treated as optimizable parameters and fit to the ab initio electrostatic potential ϕ^{QM} surrounding the molecule. Gaussian quadrupoles are defined by $l_{\max} = 2$, i.e., a Gaussian monopole, dipole, and quadrupole with the same atomic exponent parameter λ_a are placed on a given atom a. Similarly, Gaussian dipoles are defined by $l_{\max} = 1$, i.e., a Gaussian monopole and dipole with the same atomic exponent parameter λ_a are placed on a given atom a.

Points near the nuclei are either filtered out or discarded by using a weighting function $w(\vec{r})$. The weighting function $w(\vec{r})$ used in this work is a modified version of a weighting function taken from Hu et al.[60] In this present study, $w(\vec{r})$ is a sigmoid function of the form:

$$w(\vec{r}) \equiv \begin{cases} \exp\{-\sigma[\ln \rho^{QM}(\vec{r}) - \ln K_0]^2\} & \rho^{QM}(\vec{r}) \ge K_0 \\ 1 & \rho^{QM}(\vec{r}) \le K_0 \end{cases} \tag{24}$$

where ρ^{QM} is the ab initio electron density. The weighting function $w(\vec{r})$ is small for regions of high electron density, while $w(\vec{r}) = 1$ for regions of low electron density. The adjustable parameters σ and $\ln K_0$ control the curvature and the location of the sigmoid function, respectively. In the limit of large σ, $w(\vec{r})$ becomes a step function. For Gaussian multipoles, the σ and $\ln K_0$ parameters are set to 0.3 and -6.0, respectively. The σ and $\ln K_0$ parameters are selected by performing a two-dimensional (2D) scan of parameters and by observing the average error in electrostatic dimer energy of hydrogen-bonded dimers at equilibrium geometries. A plot of the average root-mean-square deviation (rmsd) error in electrostatic dimer energy is given in Figure 1 for the case of contracted ($N_c = 4$) Gaussian quadrupoles fit to the ESP calculated at the B3LYP/6-31G* level. The surface is flat, and a range of values perform equally well, e.g., (σ, $\ln K_0$) = (0.2, -7), (0.3, -6), (0.4, -5), etc. Similar parameter scans were performed with Gaussian monopoles, dipoles, and quadrupoles at various degrees of contraction N_c, and the same set of parameters were found to be local minima. In Hu et al.,[60] a weighting function for fitting atomic point charges to the ab initio ESP is proposed. There, it was shown that the point charges are stable with respect to varying

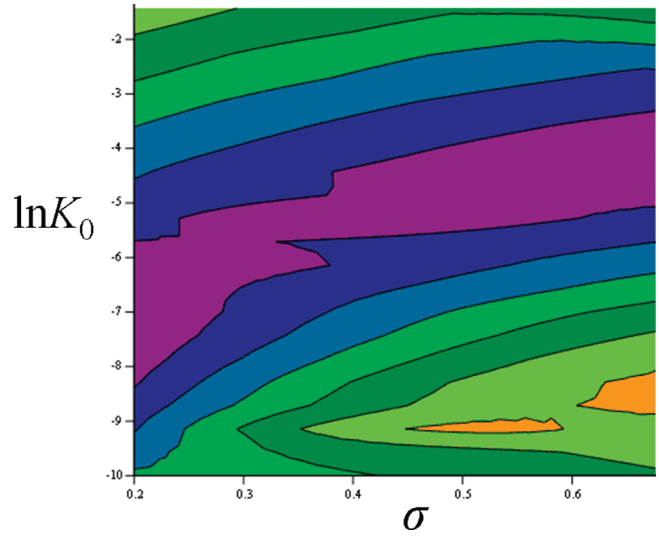

Figure 1. Contour plot of the average rmsd error in electrostatic dimer energy (kcal/mol), as a function of parameters σ and ln K_0 for the ESP weighting function $w(\vec{r})$. The electrostatic energies are calculated on hydrogen-bonded dimers at equilibrium geometries using B3LYP/6-31G* Gaussian quadrupoles ($N_c = 4$). The dark-purple running through the center represents minima in the average rmsd error in electrostatic dimer energy.

conformations. The main differences between the weighting function $w(\vec{r})$ used in this work and the one proposed by Hu[60] et al. are that the ab initio electron density ρ^{QM} is used rather than an empirical model for ρ^{QM} and that points far away from the molecule are given a weight of 1.0. We have also fit atomic point multipoles to the ESP using the σ and ln K_0 weight parameters of 0.8 and -9.0 given by Hu[60] et al.

The fitting function χ^2 is given by

$$\chi^2(Q_{lm}, \lambda) = \int d^3r w(\vec{r})[\varphi^{\mathrm{GM}}(Q_{lm}, \lambda; \vec{r}) - \varphi^{QM}(\vec{r})]^2 \tag{25}$$

where ϕ^{GM} and ϕ^{QM} are the ESPs calculated by Gaussian multipoles (eq 23) and by ab initio, respectively. χ^2 is approximated numerically on a coarse grain molecular grid taken from a modified version of NWChem[69,70] and optimized using a Levenberg−Marquardt nonlinear least-squares fit algorithm.[71] The ab initio ESP is calculated at both the B3LYP/6-31G* or HF/aug-cc-pVTZ levels using the Gaussian 03 software package.[72] Earlier in our study, we had experimented with using rectangular grids similar to the CHELPG-type[73] grids used in optimizing atomic point charges. A relatively fine grid spacing of 0.05 Å was used, and points within 1 Å of any nuclei were discarded. For uncontracted Gaussian multipole ($N_c = 1$), this procedure gave Gaussian multipole parameters which predicted electrostatic energies in approximate agreement to the results presented here, using the molecular grids with a smooth weighting function. However, for water, the number of rectangular grid points needed was on the order of 10^6-10^7, which can be compared to 10^3-10^4 grid points used in the coarse grain molecular grids.

2.4. Ab initio Dimer Energy and Molecular Density Overlap Test. The model is tested by comparing intermolecular electrostatic dimer energies and density overlap integrals on equilibrium dimer geometries of various molecules hydrogen bonded to water. The geometries of the dimers are optimized at both the B3LYP/6-31G* or HF/aug-cc-pVTZ levels, while keeping the monomers rigid in their respective monomer-optimized geometries. For the model fit to B3LYP/6-31G* data, the model is tested by comparing to the ab initio electrostatic energies calculated by the constrained space orbital variation (CSOV) decomposition[74] method, using a modified version of the HONDO[75,76] quantum chemistry program. For the model fit to HF/aug-cc-pVTZ data, ab initio electrostatic energies are calculated by the reduced variational space[77,78] (RVS) decomposition method, using the GAMESS[79] quantum chemistry program. In addition, we have developed code to calculate ab initio intermolecular density overlap integrals from the ab initio density matrix using the McMurchie−Davidson algorithm.[80]

For the water−water dimer, the model is tested by calculating intermolecular electrostatic energies and density overlap integrals on nonequilibrium dimer geometries. Several water−water dimer geometries are generated by rigidly translating one water molecule with respect to the other in the direction of the intermolecular H···O hydrogen bond. The intermolecular electrostatic energies and density overlap integrals calculated by Gaussian multipoles are plotted as a function of H···O distance and compared to their ab initio values. In addition, 100 water−water dimer geometries are generated in random orientations, while the relative center of masses lie between 2.5 and 5.0 Å. Scatter plots of the intermolecular electrostatic energy and density overlap integral are presented, comparing the results calculated by Gaussian quadrupoles with their ab initio values.

2.5. Molecular Multipole Moments. The Gaussian multipoles are further tested by comparing permanent molecular dipoles ($l = 1$), quadrupoles ($l = 2$), octapoles ($l = 3$), and hexadecapoles ($l = 4$) with their ab initio molecular multipoles. The atomic Gaussian multipole moments Q_{lm} at position $\vec{R}$ are translated to the origin by the following expression:[25]

$$Q_{lm}^{\text{origin}} = \sum_{l_1=0}^{l_{\max}} \sum_{m_1=-l_1}^{l_1} \sqrt{\binom{l+m}{l_1+m_1}\binom{l-m}{l_1-m_1}} Q_{l_1 m_1} C_{l-l_1, m-m_1}(\vec{R}) \tag{26}$$

where C_{lm} is a solid harmonic function. Note that $Q_{lm}^{\text{origin}} \neq 0$ for all values of l and m. For example, an atomic Gaussian dipole (with respect to its atomic position) contributes to the total molecular dipole, quadrupole, octapole, etc. (with respect to the origin). The translated atomic Gaussian multipoles at the origin Q_{lm}^{origin} are summed to give the total spherical tensor molecular moment. Expressions for converting real spherical tensor multipoles into traceless Cartesian multipoles can be found in Özdoğan.[81] Below, the results for converting complex spherical tensor multipoles $Q_{lm} \equiv Q^r_{lm} + iQ^i_{lm}$ into their traceless Cartesian forms are given. For $l = 1$, the Cartesian dipole μ_α is related to Q_{1m} by

$$\mu_x = -\sqrt{2}Q^r_{11} \quad \mu_y = -\sqrt{2}Q^i_{11} \quad \mu_z = Q_{10} \tag{27}$$

For $l = 2$, the traceless Cartesian quadrupoles $\Theta^{\text{TL}}_{\alpha\beta}$ are related to Q_{2m} by

$$\begin{aligned} \Theta^{\text{TL}}_{xx} &= \frac{1}{2}(-Q_{20} + \sqrt{6}Q^r_{22}) & \Theta^{\text{TL}}_{xz} &= -\sqrt{\frac{3}{2}}Q^r_{21} \\ \Theta^{\text{TL}}_{yy} &= \frac{1}{2}(-Q_{20} - \sqrt{6}Q^r_{22}) & \Theta^{\text{TL}}_{yz} &= -\sqrt{\frac{3}{2}}Q^i_{21} \\ \Theta^{\text{TL}}_{zz} &= Q_{20} & \Theta^{\text{TL}}_{xy} &= \sqrt{\frac{3}{2}}Q^r_{22} \end{aligned} \tag{28}$$

Note the trace of the quadrupoles is zero, i.e., $\text{Tr}(\Theta^{\text{TL}}) = \Theta^{\text{TL}}_{xx} + \Theta^{\text{TL}}_{yy} + \Theta^{\text{TL}}_{zz} = 0$. For the conversion formulas of traceless Cartesian octapoles ($l = 3$) and hexadecapoles ($l = 4$) from their complex spherical tensor moments, see the Supporting Information. The ab initio molecular multipole moments are calculated by Gaussian 03[72] and then converted to their traceless forms.[25] For example, the expression for converting Cartesian quadrupoles $\Theta_{\alpha\beta}$ into traceless Cartesian quadrupoles $\Theta^{\text{TL}}_{\alpha\beta}$ is given by

$$\Theta^{\text{TL}}_{\alpha\beta} = \frac{3}{2}\Theta_{\alpha\beta} - \frac{1}{2}\delta_{\alpha\beta}\sum_p \Theta_{pp} \tag{29}$$

Similar expressions for converting Cartesian octapoles and hexadecapoles into their traceless forms are given in the Supporting Information.

2.6. Gaussian Multipole Geometry Dependence. The atomic Gaussian multipole moments Q^{local}_{lm} in the local frame (eq 19) are calculated as a function of both bond length and angle for a water molecule. The geometry of water is optimized at the B3LYP/6-31G* level. Several geometries of water are found by performing two separate one-dimensional (1D) scans of perturbing one of the bond lengths and the bond angle away from equilibrium in increments of 0.1 Å and 1°, respectively. Atomic Gaussian quadrupoles Q_{lm} and exponent parameters λ ($N_c = 4$) are fit to the B3LYP/6-31G* ESP for the optimized water geometry. For each perturbed geometry, new atomic Gaussian quadrupoles are fit the B3LYP/6-31G* ESP calculated for that geometry, while the exponent parameters λ are kept at their geometry optimized values. The atomic Gaussian multipoles in the local frame Q^{local}_{lm} are plotted as a function of both bond length and angle.

2.7. Overlap−Exchange Model. The exchange−overlap model[61,62] is tested using the model for Gaussian multipole charge density for hydrogen-bonded dimer pairs. For a given dimer, several geometries are generated by translating one of the monomers in increments of 0.1 Å along the axis defined by the two atoms forming the hydrogen bond. For each dimer geometry, the B3LYP/6-31G* exchange energy E_{exch} is calculated through CSOV decomposition. Only dimer geometries for which the total dimer energy is within +5 kcal/mol of the total minimum dimer energy are kept. Typically, this entails 40−60 dimer geometries of which the exchange energy lies between 0 and 30 kcal/mol. For example, the exchange−overlap model for the water−water dimer is fit to 63 geometries, whose exchange energies lie between 0 and 27 kcal/mol. For each dimer pair, a single

molecular pair K parameter is fit to the ab initio exchange energy (eq 6), using the intermolecular density overlap integrals S calculated by Gaussian multipoles with $a = 0.95$.

3. Results

In this section, results for Gaussian monopoles, dipoles, and quadrupoles are presented. Recall that 'Gaussian quadrupoles' refers to a model in which Gaussian monopoles, dipoles, and quadrupoles with the same atomic exponent parameter λ are placed on each atom. In the next few subsections, results for intermolecular electrostatic energy, density overlap integral, and permanent molecular multipole moment, calculated by Gaussian multipoles, are compared with their respective ab initio values. For the case of water, the atomic local frame Gaussian multipole moments Q_{lm}^{local} are plotted as a function of bond length r and bond angle θ. Lastly, results are given when Gaussian multipoles are applied the exchange−overlap model.

The dependence of intermolecular electrostatic energy and density overlap integral on the degree of Slater-type contraction N_c is studied. For $N_c = 1$, the model for charge density is a single Gaussian function. In the limit of large N_c, the model for charge density is equivalent to using a Slater function $\exp(-\lambda r)$. For Gaussian multipoles fit to the B3LYP/6-31G* ESP, the results for energy and density overlap favored $N_c = 4$. However, for the Gaussian multipoles fit to the HF/aug-cc-pVTZ ESP, the errors in intermolecular electrostatic energy and density overlap decreased for larger values of N_c. The results indicate the optimal degree of contraction N_c depends on the size of the ab initio basis set. The smaller 6-31G* basis set favors a smaller degree of contraction, while the larger aug-cc-pVTZ basis set prefers a larger degree of contraction. The values of $N_c = 4$ and $N_c = 8$ are chosen for the Gaussian multipoles fit to the B3LYP/6-31G* and HF/aug-cc-pVTZ ESPs, respectively. For more details on the N_c dependence, see the Supporting Information.

3.1. Electrostatic Energy. Electrostatic dimer energies for several molecules hydrogen bonded to water are calculated at their equilibrium geometries. In Table 1, electrostatic dimer energies are given for Gaussian monopoles, dipoles, and quadrupoles with $N_c = 4$, which are fit to the ESP calculated at the B3LYP/6-31G* level. The Gaussian multipole electrostatic dimer energies are compared with their reference B3LYP/6-31G* values. The rmsd errors in the electrostatic dimer energy are 0.568, 0.567, and 0.094 kcal/mol for Gaussian monopoles, dipoles, and quadrupoles, respectively. On average, the errors for Gaussian monopoles and dipoles ($N_c = 4$) are quite similar, while a significant improvement is gained for Gaussian quadrupoles. As a representative example, the electrostatic dimer energies of the water−methanol$^{(1)}$ dimer are −8.751, −8.103, and −8.558 kcal/mol for Gaussian monopoles, dipoles, and quadrupoles, respectively. The superscript (1), (2), and (3) denote multiple dimer geometries.These numbers can be compared to the reference ab initio electrostatic energy for the water−methanol$^{(1)}$ dimer of −8.524 kcal/mol. Gaussian quadrupoles are found to be particularly important in predicting the electrostatic dimer energies of organic halides with water. For example, the ab initio electrostatic energy for the water−$CH_3Cl^{(1)}$ dimer is −0.372 kcal/mol. This result can be compared to the electrostatic dimer energies predicted by Gaussian monopoles, dipoles, and quadrupoles of −1.070, −0.719, and −0.362 kcal/mol, respectively.

Table 1. Electrostatic Energies (kcal/mol) for Equilibrium Hydrogen-Bonded Dimers (X−Water)[a]

X	E_M	E_{DM}	E_{QDM}	CSOV
formamide$^{(1)}$	−13.59	−12.82	−13.42	−13.68
formamide$^{(2)}$	−8.723	−7.849	−8.554	−8.545
formamide$^{(3)}$	−7.618	−7.089	−7.627	−7.679
N-methylformamide	−9.330	−8.058	−8.186	−8.285
water$^{(1)}$	−7.934	−7.730	−8.195	−8.235
water$^{(2)}$	−4.697	−4.582	−4.780	−4.879
water$^{(3)}$	−3.517	−3.192	−3.129	−3.179
methanol$^{(1)}$	−8.751	−8.103	−8.558	−8.524
methanol$^{(2)}$	−7.263	−7.712	−8.217	−8.296
$CH_3Cl^{(1)}$	−1.070	−0.719	−0.362	−0.372
$CH_3Cl^{(2)}$	−2.297	−2.564	−2.714	−2.768
$CH_2Cl_2^{(1)}$	−0.580	−0.274	−0.029	−0.035
$CH_2Cl_2^{(2)}$	−4.237	−4.211	−4.618	−4.693
$CH_3F^{(1)}$	−3.187	−2.731	−2.481	−2.538
$CH_3F^{(2)}$	−1.639	−1.889	−1.922	−2.003
CH_2F_2	−2.211	−1.803	−1.673	−1.743
$CH_2F_2^{(2)}$	−2.904	−3.160	−3.233	−3.358
ammonia$^{(1)}$	−10.60	−11.04	−11.95	−12.04
ammonia$^{(2)}$	−3.360	−3.263	−3.538	−3.629
methylamine	−11.61	−11.76	−12.35	−12.43
formaldehyde	−6.046	−5.330	−6.113	−6.145
acetaldehyde$^{(1)}$	−7.676	−6.762	−7.541	−7.717
acetaldehyde$^{(2)}$	−6.943	−6.156	−7.036	−7.025
acetone	−8.427	−7.541	−8.424	−8.545
dimethyl ether	−7.457	−7.849	−8.300	−8.185
rmsd	0.568	0.567	0.094	

[a] The electrostatic energies predicted by Gaussian monopoles E_M, dipoles E_{DM}, and quadrupoles E_{QDM} ($N_c = 4$) are compared to their reference B3LYP/6-31G* electrostatic dimer energies calculated using the CSOV decomposition method. The superscript (1), (2), and (3) denote multiple dimer geometries. 1 kcal/mol = 4.184 kJ/mol.

A similar analysis is performed at the HF/aug-cc-pVTZ level. Gaussian multipoles ($N_c = 8$) are fit to the ESP calculated at the HF/aug-cc-pVTZ level, while the reference ab initio electrostatic energies are calculated at the same level of theory using the RVS decomposition method. Due to computational limitations, 11 of the original 25 hydrogen-bonded dimers are studied at this level. The dimers with the smallest monomers are chosen (water, ammonia, methanol, CH_3F, and CH_2F_2). As expected, a significant improvement is found by increasing the multipole order from Gaussian monopoles to quadrupoles. The rmsd errors in electrostatic dimer energy are 0.885, 0.366, and 0.133 kcal/mol for Gaussian monopoles, dipoles, and quadrupoles, respectively. As an example, the electrostatic energies for the water−methanol$^{(1)}$ dimer predicted by Gaussian monopoles, dipoles, and quadrupoles ($N_c = 8$) are −9.233, −8.187, and −8.847 kcal/mol, respectively. These results can be compared to the HF/aug-cc-pVTZ electrostatic energy of −8.753 kcal/mol. For more individual results, see the Supporting Information.

The results for intermolecular electrostatic energy, given above, are calculated on equilibrium dimer geometries. For nonequilibrium dimer geometries, the intermolecular electrostatic energy is calculated for the water−water dimer. The

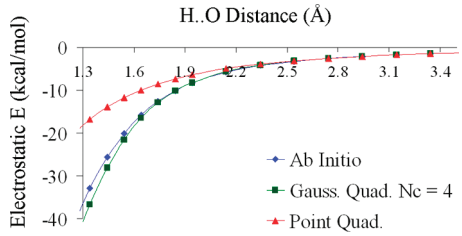

Figure 2. The electrostatic energy (kcal/mol) calculated by atomic point and Gaussian quadrupoles and by ab initio is plotted as a function of H···O distance for the water−water dimer.

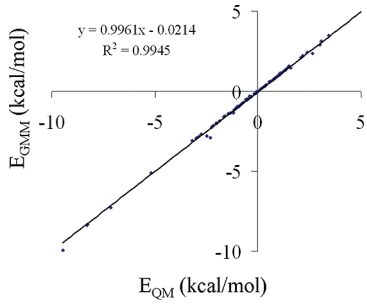

Figure 3. The intermolecular electrostatic energy (kcal/mol) calculated by Gaussian quadrupoles (*y*-axis) and by ab initio (*x*-axis) is plotted for randomly oriented water−water dimer geometries.

electrostatic energies calculated by Gaussian quadrupoles ($N_c = 4$) and by ESP-fitted atomic point quadrupoles are plotted for various hydrogen-bond distances H···O in Figure 2 for the water−water dimer and compared to their reference B3LYP/6-31G* values. As in the case of Gaussian quadrupoles, we call 'atomic point quadrupoles' as a model in which ESP-fitted atomic point monopoles, dipoles, and quadrupoles are placed on each atom. The optimized equilibrium dimer H···O distance is found to be 1.94 Å at the B3LYP/6-31G* level. At the equilibrium dimer separation, Gaussian quadrupoles predict an electrostatic energy of −8.195 kcal/mol and atomic point quadrupoles predict −6.422 kcal/mol, while the reference ab initio result is −8.235 kcal/mol. The underestimation of the atomic point quadrupole energy is an example of the penetration error[25,30,31] for atomic point multipoles. At long-range H···O distances, beyond 2.3 Å, both Gaussian and atomic point quadrupoles accurately reproduce the ab initio electrostatic energy. At short-range H···O distances, less than 1.64 Å, the Gaussian quadrupole electrostatic energy begins to slowly deviate from its reference B3LYP/6-31G* result. For example at 1.54 Å, the B3LYP/6-31G* ab initio electrostatic energy is −20.11 kcal/mol, which can be compared to the result of −21.54 kcal/mol calculated by Gaussian quadrupoles and −11.74 kcal/mol calculated by atomic point quadrupoles. In Figure 3, the intermolecular electrostatic energies calculated by Gaussian quadrupoles are compared with their ab initio reference values for several randomly oriented water−water dimers. The electrostatic energies calculated by Gaussian quadrupoles agree with their ab initio reference values for energies ranging from −10 kcal/mol to +5 kcal/mol. Additional scatter plots of intermolecular electrostatic energy can be found in the Supporting Information for randomly oriented hydrogen-bonded dimers.

In order to compare Gaussian multipoles with the Gaussian Electrostatic Model (GEM),[57] electrostatic dimer energies are calculated on 10 water dimers,[82,83] which represent local minima on the water−water potential energy surface. Previously, GEM[57] was fit to the B3LYP/6-31G* ESP using the A1 and P1 auxiliary Gaussian basis sets (ABS). Two GEM models for water were developed. In a three-point GEM water model, ABS's have been placed on atomic centers only. A second GEM water model has been developed by placing ABS's on both the atomic centers and the bond midpoints, resulting in a five-point GEM water model. The average absolute errors in the electrostatic energy for the three-point GEM water model are 0.11 and 0.12 kcal/mol for the A1 and P1 basis sets, respectively. Including basis functions on bond midpoints results in an improved fit for GEM. The errors in the five-point GEM water fit to the ESP are 0.06 and 0.04 kcal/mol for the A1 and P1 basis sets, respectively. The average errors in electrostatic dimer energy for GEM can be compared to the error of 0.06 kcal/mol for Gaussian quadrupoles ($N_c = 4$). The GEM five-point water model with the A1 and P1 basis sets have a total of 110 and 213 primitive Gaussian functions, respectively. The total number of uncontracted basis functions in the GEM water models can be compared to the total number of contracted Gaussian quadrupoles of 27.

3.2. Molecular Density Overlap Integral. The model for Gaussian multipoles is further tested by comparing intermolecular density overlap integrals with their ab initio values. In Table 2, the intermolecular density overlap integrals are given for the hydrogen-bonded dimers at their equilibrium geometries. The intermolecular density overlap integrals for Gaussian monopoles, dipoles, and quadrupoles ($N_c = 4$) are compared with their respective B3LYP/6-31G* values. On average, there is a significant improvement in going up in multipole order from Gaussian monopoles to quadrupoles. The rmsd errors in intermolecular density overlap integrals are 2.571-, 0.752-, and 0.195 × 10^{-3} $e^2/Å^3$ for Gaussian monopoles, dipoles, and quadrupoles, respectively. A representative example is the water−methylamine complex at equilibrium, which has an ab initio value of 15.89 × 10^{-3} $e^2/Å^3$. This value can be compared to the intermolecular density overlap calculated by Gaussian monopoles, dipoles, and quadrupoles of 19.78-, 17.05-, and 15.56 × 10^{-3} $e^2/Å^3$, respectively. Similar trends can be found for the Gaussian multipoles fit to the HF/aug-cc-pVTZ ESP. At the HF/aug-cc-pVTZ level, the rmsd errors in intermolecular density overlap integral are 2.668-, 0.502-, and 0.268 × 10^{-3} $e^2/Å^3$ for Gaussian monopoles, dipoles, and quadrupoles ($N_c = 8$), respectively. For individual results on HF/aug-cc-pVTZ Gaussian multipoles, see the Supporting Information.

The results given in Table 2 are for intermolecular density overlap integrals calculated at equilibrium dimer distances. For nonequilibrium dimer geometries, the intermolecular density overlap integrals are compared with their ab initio values for the water−water dimer. In Figure 4, the intermolecular density overlap integrals calculated by B3LYP/6-31G* Gaussian quadrupoles ($N_c = 4$) and the B3LYP/6-31G*

Table 2. Intermolecular Density Overlap Integrals ($\times 10^{-3}$ e^2/Å^3) for Equilibrium Hydrogen-Bonded Dimers (X−Water)[a]

X	S_M	S_{DM}	S_{QDM}	S_{QM}
formamide(1)	20.29	17.30	16.76	16.99
formamide(2)	15.47	11.05	11.25	10.88
formamide(3)	8.283	7.201	7.577	7.399
N-methylformamide	16.36	12.04	11.43	11.37
water(1)	11.28	9.969	9.133	9.061
water(2)	2.871	2.513	2.503	2.698
water(3)	1.189	0.958	0.930	1.084
methanol(1)	15.40	12.70	11.47	11.30
methanol(2)	8.783	10.21	9.470	9.518
CH_3Cl(1)	0.662	0.461	0.243	0.308
CH_3Cl(2)	1.790	2.469	3.238	3.250
CH_2Cl_2(1)	0.329	0.217	0.116	0.162
CH_2Cl_2(2)	3.812	3.704	5.341	5.440
CH_3F(1)	5.679	3.358	2.886	3.086
CH_3F(2)	2.542	2.561	2.738	2.881
CH_2F_2(1)	3.635	2.044	1.806	2.036
CH_2F_2(2)	4.477	4.016	4.275	4.569
ammonia(1)	15.63	13.75	13.21	13.39
ammonia(2)	3.647	4.297	4.230	4.327
methylamine	19.78	17.05	15.56	15.89
formaldehyde	10.71	8.028	8.060	7.871
acetaldehyde(1)	12.77	9.957	9.584	9.657
acetaldehyde(2)	12.63	9.390	9.573	9.241
acetone	14.30	11.37	11.18	11.12
dimethyl ether	15.56	14.34	12.58	12.25
rmsd	2.571	0.752	0.195	

[a] The overlap integrals predicted by Gaussian monopoles S_M, dipoles S_{DM}, and quadrupoles S_{QDM} ($N_c = 4$) are compared to their reference B3LYP/6-31G* values. The superscripts (1), (2), and (3) denotes multiple dimer geometries. 10^{-3} e^2/Å^3 = 1.482 $\times$ 10^{-4} e^2/a_0^3, where a_0 is the Bohr radius.

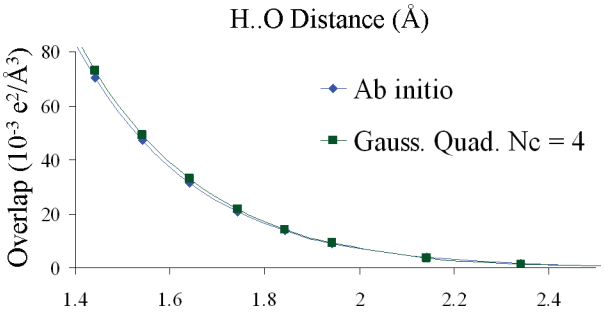

Figure 4. The intermolecular density overlap integral ($\times$ 10^{-3} e^2/Å^3) calculated by atomic Gaussian quadrupoles and by ab initio is plotted as a function of H···O distance (Å) for the water−water dimer.

reference values are plotted as a function of H···O distance. The intermolecular overlap integrals predicted by Gaussian quadrupoles agree with their ab initio values for H···O distances ranging from 2.3 to 1.7 Å. For shorter separations, the intermolecular overlap integrals predicted by Gaussian quadrupoles begin to overestimate the ab initio result. In Figure 5, the intermolecular density overlap integral calculated by Gaussian quadrupoles is compared with its respective ab initio value for several randomly oriented water−water geometries. The intermolecular overlap integrals range from 0 to 30.0 $\times$ 10^{-3} e^2/Å^3. There is a small overestimation (~6%) of the intermolecular density overlap integrals calculated by Gaussian quadrupoles as compared with their ab initio values. In the Supporting Information, additional

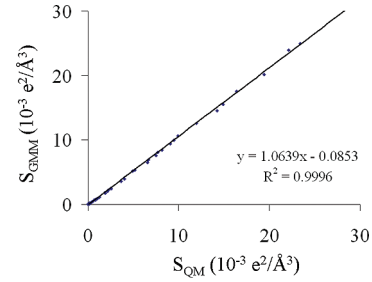

Figure 5. The intermolecular density overlap integral ($\times$ 10^{-3} e^2/Å^3) calculated by Gaussian quadrupoles (*y*-axis) and by ab initio (*x*-axis) is plotted for randomly oriented water−water dimer geometries.

Table 3. Non-Zero Components of the Molecular Quadrupole Moment D-Å of Ammonia for Gaussian Monopoles, Dipoles, And Quadrupoles ($N_c = 4$) Fit to B3LYP/6-31G* ESP

atomic	*xx*	*yy*	*zz*	rmsd
Gaussian monopoles	0.9211	0.9211	−1.8422	0.39291
Gaussian dipoles	1.2701	1.2700	−2.5400	0.04402
Gaussian quadrupoles	1.3139	1.3138	−2.6278	0.00015
B3LYP/6-31G*	1.3140	1.3140	−2.6281	

Table 4. Average Rmsd Error (Δ) in Traceless Molecular Dipole, Quadrupole, Octapole, and Hexadecapole Moments[a]

atomic	Δdip (10^{-3} D)	Δquad (D-Å)	Δoct (D-Å^2)	Δhex (D-Å^3)
Gaussian monopoles	9.489	0.1947	0.9970	3.402
Gaussian dipoles	2.495	0.0453	0.2154	0.969
Gaussian quadrupoles	1.045	0.0061	0.0381	0.130

[a] Averaged over 14 molecules for Gaussian multipoles ($N_c = 4$) fit to the B3LYP/6-31G* ESP.

scatter plots of intermolecular density overlap integral can be found for other randomly oriented hydrogen bonded dimers.

3.3. Molecular Multipole Moments. The permanent molecular multipole moments up to hexadecapole are calculated for the atomic Gaussian monopole, dipole, and quadrupole models ($N_c = 4$) and compared with their reference B3LYP/6-31G* values. As an example, the nonzero components of the molecular quadrupole for ammonia are given in Table 3. A significant improvement is found by increasing the atomic Gaussian multipole order from Gaussian monopoles to quadrupoles. For example, the ab initio Q_{xx} component of the molecular quadrupole is 1.3140 D-Å, which can be compared to the value predicted by Gaussian monopoles, dipoles, and quadrupoles of 0.9211, 1.2701, and 1.3139 D-Å, respectively.

The results for molecular multipole moments given for ammonia are representative of the other 14 monomers studied in this work. The rmsd errors in molecular multipole moment up to hexadecapole are averaged over all the molecules and presented in Table 4. As expected, there is a significant decrease in average rmsd error for increasing atomic Gaussian multipole order. For example, the average rmsd errors in molecular hexadecapole are 3.402 for atomic Gaussian monopoles, 0.969 for Gaussian dipoles, and 0.130 D-Å^3 for

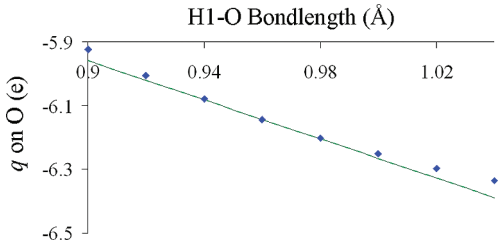

Figure 6. Atomic Gaussian monopole moment q (e) on oxygen in a water molecule as a function of H1−O bond length. The B3LYP/6-31G* equilibrium H1−O bond length is 0.9684 Å.

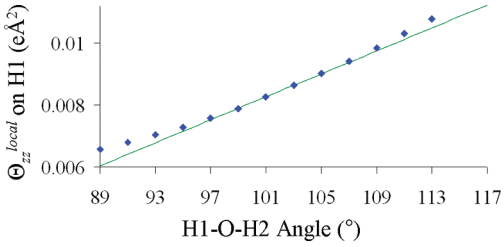

Figure 7. Atomic local frame Gaussian quadrupole moment Θ_{zz}^{local} (eÅ^2) on the 'H1' hydrogen in a water molecule as a function of H1−O−H2 bond angle. The B3LYP/6-31G* equilibrium H1−O−H2 bond angle is 103.66°.

Gaussian quadrupoles. For more individual results, see the Supporting Information.

3.4. Gaussian Multipole Geometry Dependence. The atomic Gaussian multipole moments are investigated as a function of bond length r and bond angle θ for the case of water. Gaussian quadrupoles ($N_c = 4$) are calculated at the B3LYP/6-31G* level for several geometries of water obtained by perturbing either the O−H1 bond length or the H1−O−H2 bond angle. The atomic Gaussian multipole moments in the local frame (eq 19) are converted to their traceless Cartesian moments (eqs 27 and 28). In Figure 6, the atomic Gaussian monopole moment q on oxygen is plotted when the H1−O bond length is varied. The Gaussian monopole charge q is a smooth function of bond length, which can be approximated as a straight line for bond lengths between 0.92 and 1.00 Å (the equilibrium bond length is 0.9684 Å). In addition, the zz component of the local frame traceless Cartesian quadrupole moment Θ_{zz}^{local} on the H1 hydrogen is plotted as a function of H1−O−H2 bond angle in Figure 7. Θ_{zz}^{local} can be approximated as a straight line for bond angles between 95° and 111° (the equilibrium bond angle is 103.66°). In both Figures 6 and 7, the straight lines are determined by the value of the local frame atomic multipoles Q_{lm}^{local} at the equilibrium geometry and by the finite difference derivative of Q_{lm}^{local} with respect to the bond length or bond angle at the equilibrium geometry. The results given in Figures 6 and 7 are examples, and the other atomic Gaussian moments Q_{lm}^{local} follow similar trends (see the Supporting Information for more examples). For small internal geometry perturbations, the above results suggest that the local frame atomic Gaussian multipole moments can be approximated by a truncated linear Taylor series as a function of the two bond lengths r_1 (H1−O) and r_2 (H2−O) and the bond angle θ (H1−O−H2) as

$$Q_{lm}^{local}(r,\theta) \cong Q_{lm}^{local,0} + (r_1 - r_1^0)\frac{\partial Q_{lm}^{local,0}}{\partial r_1} + (r_2 - r_2^0)\frac{\partial Q_{lm}^{local,0}}{\partial r_2} + (\theta - \theta^0)\frac{\partial Q_{lm}^{local,0}}{\partial \theta} \quad (29)$$

where $Q_{lm}^{local,0}$ is the atomic Gaussian multipole at the geometry optimized equilibrium structure. Evaluated at the equilibrium structure, $\partial Q_{lm}^{local,0}/\partial r_1$, $\partial Q_{lm}^{local,0}/\partial r_2$, and $\partial Q_{lm}^{local,0}/\partial \theta$ are the finite difference partial derivatives of $Q_{lm}^{local,0}$ with respect to r_1, r_2, and θ, respectively.

3.5. Exchange−Overlap Model. The exchange−overlap model is fit to exchange−repulsion energies calculated at the B3LYP/6-31G* level through CSOV decomposition as described in Section 2.7. The intermolecular density overlap integrals are calculated from Gaussian quadrupoles ($N_c = 4$) fit to the B3LYP/6-31G* ESP. For the water−water dimer, the rmsd error of fit is 0.350 kcal/mol for Gaussian quadrupoles, over a range of exchange energies from 0.0 to 27.0 kcal/mol. At the equilibrium water−water dimer distance, the exchange energy calculated by the exchange−overlap model is 5.449 kcal/mol, compared to the ab initio result of 5.362 kcal/mol. In Figure 8, the water−water exchange energy calculated by the model is compared with the ab initio value and plotted as a function of H···O distance. A similar analysis is performed on the other hydrogen-bonded dimers. The rmsd fit errors are averaged over all the dimers and given by 0.764, 0.379, and 0.275 kcal/mol for Gaussian monopoles, dipoles, and quadrupoles, respectively. This result indicates that including anisotropy into the model for charge density makes a significant improvement when applying the exchange−overlap model. At equilibrium distances, the exchange energies lie between 0.1 and 10 kcal/mol. The rmsd in exchange energy at the equilibrium dimer distance averaged over the hydrogen-bonded dimers are 1.782, 0.262, and 0.276 kcal/mol for Gaussian monopoles, dipoles, and quadrupoles, respectively. For Gaussian quadrupoles, the molecular pair K parameters range from 0.5786 kcal/mol ($\times$ 10^3 Å^3/e^2)$^{0.95}$ for the water−CH_3F dimer to 0.7499 for the water−ammonia dimer. The average value of the molecular pair K parameter over all the dimers is 0.6607. Because of the variability of the K parameters, a single molecular pair K parameter may not be sufficient for larger molecules or for when a large amount of configuration space is sampled. For more individual

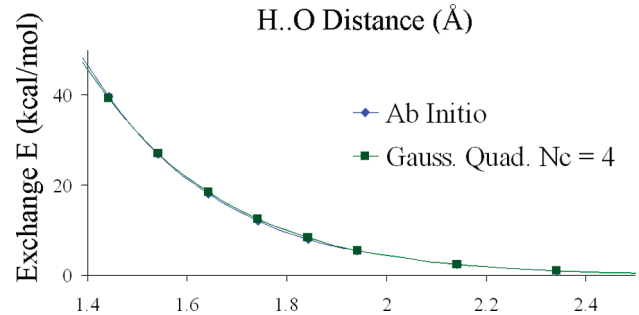

Figure 8. The exchange energy calculated by Gaussian quadrupoles and by ab initio is plotted as a function of H···O distance for the water−water dimer.

results, including exchange parameters K, rmsd errors, and exchange dimer energies, see the Supporting Information.

4. Conclusion

We have proposed a model based on contracted Gaussian multipole charge density. The atomic Gaussian multipoles are fit to the ab initio electrostatic potential and are shown to reproduce ab initio electrostatic dimer energies, intermolecular density overlap integrals, and permanent molecular multipole moments. For the case of water, the local frame atomic Gaussian multipole moments Q_{lm}^{local} are shown to be a smooth function of bond length r and bond angle θ, which can be approximated as a truncated linear Taylor series. In a follow up work, we will present analytic atomic force expressions for geometry-dependent Gaussian multipoles and show that geometry-dependent electrostatic models are capable of reproducing ab initio electrostatic atomic forces. In addition, the intermolecular density overlap integrals calculated by Gaussian multipoles have been applied to a model[61,62] for exchange−repulsion energy based on intermolecular density overlap integral. A molecular pair K parameter is fit to the ab initio exchange−repulsion energy for hydrogen-bonded dimers. A significant improvement is found in going from Gaussian monopoles to quadrupoles, indicating that including anisotropy in the description of atomic charge density is important. Though the preliminary results of applying the exchange−overlap model to the Gaussian multipole charge density are encouraging, a more extensive investigation would be useful, possibly by studying atomic pair K parameters fit to a larger molecular data set. We plan to further study the exchange−overlap model using Gaussian multipoles, and we hope to propose a general set of transferable exchange−overlap parameters in the near future.

Acknowledgment. This research was supported in part by the Intramural Research Program of the National Institute of Health (NIH) and the National Institute of Environmental Health Sciences (Z01 ES9043010-23). L.G.P. acknowledges support from the National Science Foundation Focused Research Groups, Department of Materials Research 0804549 and from the NIH L06350. We would like to thank the reviewers for their helpful comments, which improved the manuscript.

Supporting Information Available: There are three parts available. Part I contains additional mathematical details and background. Elementary properties of spherical, solid, and scaled solid harmonic functions are given along with some theorems for the solid harmonic function and the solid harmonic gradient operator. Expressions for electrostatic energy and density overlap integral are derived for complex Gaussian multipoles along with the Cartesian gradients of their matrix elements. In addition, formulas for converting complex spherical tensor multipole moments into their traceless Cartesian forms are given. In part II, additional results for Gaussian multipoles are presented. The dependence on the degree of Slater-type contraction N_c is discussed. Additional tables and figures of electrostatic dimer energies and intermolecular density overlap integrals are presented. For the case of water, additional plots of Q_{lm}^{local} as a function of bond length and bond angle are given. For the exchange−overlap model, exchange−repulsion energies, molecular pair K parameters, and rmsd of fits are provided for B3LYP/6-31G* Gaussian multipoles. In part III, the Gaussian multipole parameters, the Slater-type contraction coefficients/exponents, and the equilibrium dimer geometries are given. This material is available free of charge via the Internet at http://pubs.acs.org.

References

(1) Thole, B. T. *Chem. Phys.* **1981**, *59*, 341–350.

(2) Elking, D. M.; Darden, T.; Woods, R. J. *J. Comput. Chem.* **2007**, *28*, 1261–1274.

(3) Lamoureux, G.; MacKerell, A. D.; Roux, B. *J. Chem. Phys.* **2003**, *119* (10), 5185–5197.

(4) Rick, S. W.; Stuart, S. J.; Berne, B. J. *J. Chem. Phys.* **1994**, *101* (7), 6141–6156.

(5) Stern, H. A.; Kaminski, G. A.; Banks, J. L.; Zhou, R.; Berne, B. J.; Friesner, R. *J. Phys. Chem.* **1999**, *103*, 4730–4737.

(6) Piquemal, J.-P.; Chelli, R.; Procacci, P.; Gresh, N. *J. Phys. Chem. A* **2007**, *111*, 8170–8176.

(7) Patel, S.; Brooks, C. L., III *J. Comput. Chem.* **2004**, *25*, 1–16.

(8) Patel, S.; MacKerell, A. D.; Brooks III, C. L. *J. Comput. Chem.* **2004**, *25*, 1504–1514.

(9) Kaminski, G. A.; Stern, H. A.; Berne, B. J.; Friesner, R. *J. Phys. Chem. A* **2004**, *108*, 621–627.

(10) Gresh, N.; Cisneros, G. A.; Darden, T. A.; Piquemal, J.-P. *J. Chem. Theory Comput.* **2007**, *3*, 1960–1986.

(11) Gresh, N. *J. Comput. Chem.* **1995**, *16*, 856–882.

(12) Piquemal, J-P; Chevreau, H.; Gresh, N. *J. Chem. Theory Comput.* **2007**, *3*, 824–837.

(13) Ren, P.; Ponder, J. W. *J. Phys. Chem. B* **2003**, *107*, 5933–5947.

(14) Ren, P.; Ponder, J. W. *J. Comput. Chem.* **2002**, *23*, 1497–1506.

(15) Grossfield, A.; Ren, P.; Ponder, J. W. *J. Am. Chem. Soc.* **2003**, *125*, 15671–15682.

(16) Piquemal, J.-P.; Perera, L.; Cisneros, G. A.; Ren, P.; Pedersen, L. G.; Darden, T. A. *J. Chem. Phys.* **2006**, *125*, 054511.

(17) Iuchi, S.; Izvekov, S.; Voth, G. A. *J. Chem. Phys.* **2007**, *126*, 124505–124512.

(18) Paesani, F.; Iuchi, S.; Voth, G. A. *J. Chem. Phys.* **2007**, *127* (7), 074506−074515.

(19) Wang, F.; Jordan, K. D. *J. Chem. Phys.* **2002**, *116*, 6973–6981.

(20) Jiang, H.; Jordan, K. D.; Taylor, C. E. *J. Phys. Chem. B* **2007**, *111*, 6486–6492.

(21) Koch, U.; Popelier, P. L. A.; Stone, A. J. *Chem. Phys. Lett.* **1995**, *2*, 253–260.

(22) Koch, U.; Stone, A. J. *J. Chem. Soc., Faraday Trans.* **1996**, *92* (10), 1701–1708.

(23) Cho, K.; Kang, Y. K.; No, K. T.; Scheraga, H. A. *J. Phys. Chem. B* **2001**, *105*, 3624–3634.

(24) Mankoo, P.; Keyes, T. *J. Chem. Phys.* **2008**, *129*, 034504−034509.

(25) Stone, A. J. *The Theory of Intermolecular Forces*; Oxford University Press: Oxford, U.K., 2000.

(26) Stone, A. J. *Chem. Phys. Lett.* **1981**, *83*, 233–239.

(27) Vigné-Maeder, F.; Claverie, P. *J. Chem. Phys.* **1998**, *88*, 4934–4948.

(28) Náray-Szabó, G; Ferenczy, G. G. *Chem. Rev.* **1995**, *95* (4), 829–847.

(29) Ángyán, J. G.; Chipot, C.; Dehez, F.; Hättig, C.; Jansen, G.; Millot, C. *J. Comput. Chem.* **2003**, *24*, 997–1008.

(30) Qian, W.; Krimm, S. *J. Phys. Chem. A* **2005**, *109*, 5608–5618.

(31) Freitag, M. A.; Gordon, M. S.; Jensen, J. H.; Stevens, W. J. *J. Chem. Phys.* **2000**, *112* (17), 7300–7306.

(32) Piquemal, J-P; Gresh, N.; Giessner-Prettre, C. *J. Phys. Chem. A* **2003**, *107*, 10353–10359.

(33) Cisneros, G. A.; Tholander, S. Na-Im; Elking, D. M.; Darden, T. A.; Parisel, O.; Piquemal, J-P *Int. J. Quantum Chem.* **2008**, *108*, 1905–1912.

(34) Slipchenko, L. V; Gordon, M. S. *Mol. Phys.* **2009**, *107*, 999–1016.

(35) Chelli, R.; Righini, R.; Califano, S.; Procacci, P. *J. Mol. Liq.* **2002**, *96*−*97*, 87–100.

(36) Masia, M.; Probst, M.; Rey, R. *J. Chem. Phys.* **2005**, *123*, 164505–13.

(37) Paricaud, P.; Předota, M.; Chialvo, A.; Cummings, P. *J. Chem. Phys.* **2005**, *122*, 244511–244514.

(38) Wheatley, R. J. *Mol. Phys.* **1993**, *79*, 597–610.

(39) Wheatley, R. J.; Mitchell, J. B. O. *J. Comput. Chem.* **1994**, *15*, 1187–1198.

(40) Hall, G. G. *Adv. At. Mol. Phys.* **1985**, *20*, 41–63.

(41) Martin, D.; Hall, G. G. *Theor. Chim. Acta* **1981**, *59*, 281–290.

(42) Giese, T. J.; York, D. M. *J. Chem. Phys.* **2008**, *128* (6), 064104−6.

(43) Hobson, E. W. *The Theory of Spherical and Ellipsoidal Harmonics*; Chelsea: New York, 1955, pp 93.

(44) Bayman, B. F. *J. Math. Phys.* **1978**, *19*, 2558–2562.

(45) Chakrabarti, S.; Dewangan, D. P. *J. Phys. B: At. Mol. Opt. Phys.* **1995**, *28*, L769–774.

(46) Helgaker, T.; Jorgensen, P.; Olsen, J. *Molecular Electronic-Structure Theory*; Wiley: Chichester, U.K., 2004, pp. 337−424.

(47) Arken, G. B. *Mathematical Methods for Physicists*, 5th ed.; Academic Press: San Diego, CA, 2000, pp 693−765.

(48) Cisneros, G. A.; Piquemal, J.-P.; Darden, T. A. *J. Chem. Phys.* **2005**, *123*, 044109−044110.

(49) Cisneros, G. A.; Piquemal, J.-P.; Darden, T. A. *J. Chem. Phys.* **2006**, *125* (18), 184101–184116.

(50) Piquemal, J.-P.; Cisneros, G. A.; Reinhardt, P.; Gresh, N.; Darden, T. A. *J. Chem. Phys.* **2006**, *124* (10), 104101–104112.

(51) Cisneros, G. A.; Darden, T. A.; Gresh, N.; Reinhardt, P.; Parisel, O.; Pilmé, J.; Piquemal, J.-P. Design of Next Generation Force Fields from Ab Initio Computations: Beyond Point Charges. In *Electrostatics Multi-scale Quantum Models for Biocatalysis: Modern Techniques and Applications, for the Book Series: Challenges and Advances in Computational Chemistry and Physics*; York, D. M., Lee, T.-S., Eds.; Springer Verlag: New Amsterdam, The Netherlands, 2009; Vol. 7, pp 137−172.

(52) Dunlap, B. I.; Connolly, W. D.; Sabin, J. R. *J. Chem. Phys.* **1979**, *71*, 4993–4999.

(53) Köster, A. M. *J. Chem. Phys.* **1996**, *104*, 4114–4124.

(54) Köster, A. M. *J. Chem. Phys.* **2003**, *118*, 9943–9951.

(55) Eichkorn, K.; Treutler, O.; Ohm, H.; Haser, M.; Ahlrichs, R. *Chem. Phys. Lett.* **1995**, *240*, 283–289.

(56) Jung, Y; Sodt, A; Gill, P. M. W. Gill; Head-Gordon, M. *Proc. Natl. Acad. Sci. U.S.A.* **2005**, *102*, 6692−6697.

(57) Cisneros, G. A.; Elking, D. M.; Piquemal, J-P; Darden, T. A. *J. Phys. Chem. A* **2007**, *111*, 12049–12056.

(58) Hehre, W. J.; Stewart, R. F.; Pople, J. A. *J. Chem. Phys.* **1969**, *51* (6), 2657–2664.

(59) Stewart, R. F. *J. Chem. Phys.* **1970**, *52* (1), 431–438.

(60) Hu, H; Lu, Z; Yang, W. *J. Chem. Theory Comput.* **2007**, *3*, 1004–1013.

(61) Wheatley, R. J.; Price, S. L. *Mol. Phys.* **1990**, *69*, 507–533.

(62) Mitchell, J. B. O.; Price, S. L. *J. Phys. Chem. A* **2000**, *104*, 10958–10971.

(63) Dunlap, B. I. *Phys. Rev. A: At., Mol., Opt. Phys.* **1990**, *42* (3), 1127–1137.

(64) Dunlap, B. I. *Int. J. Quantum Chem.* **2001**, *81*, 373–383.

(65) Dunlap, B. I. *J. Chem. Phys.* **2003**, *118* (3), 1036–1043.

(66) Choi, C. H.; Ivanic, J.; Gordon, M. S.; Ruedenberg, K. *J. Chem. Phys.* **1999**, *11*, 8825–8831.

(67) Toukmaji, A.; Sagui, C.; Board, J. A.; Darden, T. A. *J. Chem. Phys.* **2000**, *113*, 10913–10927.

(68) Sagui, C.; Pedersen, L. G.; Darden, T. A. *J. Chem. Phys.* **2004**, *120*, 73–87.

(69) Bylaska, E. J.; de Jong, W. A.; Govind, N.; Kowalski, K.; Straatsma, T. P.; Valiev, M.; Wang, D.; Apra, E.; Windus, T. L.; Hammond, J.; Nichols, P.; Hirata, S.; Hackler, M. T.; Zhao, Y.; Fan, P.-D.; Harrison, R. J.; Dupuis, M.; Smith, D. M. A.; Nieplocha, J.; Tipparaju, V.; Krishnan, M.; Wu, Q.; Van Voorhis, T.; Auer, A. A.; Nooijen, M.; Brown, E.; Cisneros, G.; Fann, G. I.; Fruchtl, H.; Garza, J.; Hirao, K.; Kendall, R.; Nichols, J. A.; Tsemekhman, K.; Wolinski, K.; Anchell, J.; Bernholdt, D.; Borowski, P.; Clark, T.; Clerc, D.; Dachsel, H.; Deegan, M.; Dyall, K.; Elwood, D.; Glendening, E.; Gutowski, M.; Hess, A.; Jaffe, J., Johnson, B.; Ju, J.; Kobayashi, R.; Kutteh, R.; Lin, Z.; Littlefield, R.; Long, X.; Meng, B.; Nakajima, T.; Niu, S.; Pollack, L.; Rosing, M.; Sandrone, G.; Stave, M.; Taylor, H.; Thomas, G.; van Lenthe, J.; Wong, A.; Zhang, Z. *NWChem, A Computational Chemistry Package for Parallel Computers*, version 5.1(a modified version); Pacific Northwest National Laboratory: Richland, WA, 2007.

(70) Kendall, R. A.; AprÃ, E.; Bernholdt, D. E.; Bylaska, E. J.; Dupuis, M.; Fann, G. I.; Harrison, R. J.; Ju, J.; Nichols, J. A.; Nieplocha, J.; Straatsma, T. P.; Windus, T. L.; Wong, A. T. High Performance Computational Chemistry: an Overview of NWChem a Distributed Parallel Application. *Comput. Phys. Commun.* **2000**, *128*, 260–283.

(71) Press, W. H.; Flannery, B. P.; Teukolsky, S. A.; Vetterling, W. T. *Numerical Recipes in C: The Art of Scientific*

Computing, 2nd ed.; Cambridge University Press: Cambridge, 1992; p. 683.

(72) Frisch, M. J.; Trucks, G. W.; Schlegel, H. B.; Scuseria, G. E.; Robb, M. A.; Cheeseman, J. R.; Montgomery, Jr., J. A.; Vreven, T.; Kudin, K. N.; Burant, J. C.; Millam, J. M.; Iyengar, S. S.; Tomasi, J.; Barone, V.; Mennucci, B.; Cossi, M.; Scalmani, G.; Rega, N.; Petersson, G. A.; Nakatsuji, H.; Hada, M.; Ehara, M.; Toyota, K.; Fukuda, R.; Hasegawa, J.; Ishida, M.; Nakajima, T.; Honda, Y.; Kitao, O.; Nakai, H.; Klene, M.; Li, X.; Knox, J. E.; Hratchian, H. P.; Cross, J. B.; Bakken, V.; Adamo, C.; Jaramillo, J.; Gomperts, R.; Stratmann, R. E.; Yazyev, O.; Austin, A. J.; Cammi, R.; Pomelli, C.; Ochterski, J. W.; Ayala, P. Y.; Morokuma, K.; Voth, G. A.; Salvador, P.; Dannenberg, J. J.; Zakrzewski, V. G.; Dapprich, S.; Daniels, A. D.; Strain, M. C.; Farkas, O.; Malick, D. K.; Rabuck, A. D.; Raghavachari, K.; Foresman, J. B.; Ortiz, J. V.; Cui, Q.; Baboul, A. G.; Clifford, S.; Cioslowski, J.; Stefanov, B. B.; Liu, G.; Liashenko, A.; Piskorz, P.; Komaromi, I.; Martin, R. L.; Fox, D. J.; Keith, T.; Al-Laham, M. A.; Peng, C. Y.; Nanayakkara, A.; Challacombe, M.; Gill, P. M. W.; Johnson, B.; Chen, W.; Wong, M. W.; Gonzalez, C.; and Pople, J. A. *Gaussian 03, Revision C.02*; Gaussian, Inc.: Wallingford, CT, 2004.

(73) Breneman, C. M.; Wiberg, K. B. *J. Comput. Chem.* **1990**, *11*, 361–373.

(74) Bagus, P. S.; Hermann, K.; Bauschlicher, C. W., Jr. *J. Chem. Phys.* **1984**, *80*, 4378–4386.

(75) Piquemal, J.-P.; Marquez, A.; Parisel, O.; Giessner-Prettre, C. *J. Comput. Chem.* **2005**, *26*, 1052–1062.

(76) Dupuis, M.; Marquez, A.; Davidson, E. R. *HONDO95.3*; Indiana University: Bloomington, IN, 1995.

(77) Stevens, W. J; Fink, W. H. *Chem. Phys. Lett.* **1987**, *139* (1), 15–22.

(78) Chen, W.; Gordon, M. S. *J. Phys. Chem.* **1996**, *100*, 14316–14328.

(79) Schmidt, M. W.; Baldridge, K. K.; Boatz, J. A.; Elbert, S. T.; Gordon, M. S.; Jensen, J. J.; Koseki, S.; Matsunaga, N.; Nguyen, K. A.; Su, S.; Windus, T. L.; Dupuis, M.; Montgomery, J. A. *J. Comput. Chem.* **1993**, *4*, 1347.

(80) McMurchie, L. E.; Davidson, E. R. *J. Comp. Phys.* **1978**, *26*, 218–231.

(81) Özdoğan, T. *J. Math. Chem.* **2006**, *42* (2), 201–214.

(82) Tschumper, G. S.; Leininger, M. L.; Hoffman, B. C.; Valeev, E. F.; Schaffer, H. F.; Quack, M. *J. Chem. Phys.* **2002**, *116*, 690–701.

(83) van Duijneveldt-van, de; Rijdt, J. G. C. M.; Mooij, W. T. M.; Duijneveldt, F. B *Phys. Chem. Chem. Phys.* **2003**, *5*, 1169–1180.

CT900348B